Quaternary Science Reviews 126 (2015) 254–263

Contents lists available at ScienceDirect

Quaternary Science Reviews

journal homepage: www.elsevier.com/locate/quascirev

Southern Westerly Winds submit to the ENSO regime: A multiproxy paleohydrology record from Lake Dobson, Tasmania

Andrew B.H. Rees [a, b, *], Les C. Cwynar [a], Michael-Shawn Fletcher [c]

[a] Department of Biology, University of New Brunswick, Fredericton, New Brunswick E3B 5A3, Canada
[b] School of Geography, Environment and Earth Sciences, Victoria University of Wellington, Wellington 6012, New Zealand
[c] School of Geography, Faculty of Science, University of Melbourne, Melbourne, VIC 3010, Australia

ARTICLE INFO

Article history:
Received 22 April 2015
Received in revised form
18 August 2015
Accepted 19 August 2015
Available online 18 September 2015

Keywords:
ENSO
Southern Westerly Winds
Paleohydrology
Fire
Charcoal
Chironomids
Itrax
Holocene

ABSTRACT

The El Niño-Southern Oscillation (ENSO) and Southern Westerly Winds (SWW) profoundly influence synoptic-scale climate in the Southern Hemisphere. Although many studies have invoked either phenomenon to explain trends in proxy data, few have demonstrated the transition from a climate dominated by SWW flow to one controlled by El Niño activity, which is postulated to have occurred after 5 cal ka BP in the mid-latitudes of the Southern Hemisphere. Tasmania, southeast Australia, is ideally situated to detect changes in both of these climatic controls. Currently, El Niño and La Niña events result in drier and wetter conditions island-wide, respectively, with the greatest impact in the north. Further, Tasmania houses north–south trending mountain ranges near its western coast. As a result, areas west of the mountains exhibit a positive correlation between SWW flow and precipitation, while eastern regions possess either no or a negative relationship. Here, we present data from chironomid remains, charcoal, and geochemical proxies to investigate the paleohydrological history of Lake Dobson, a site located in Mount Field National Park, Tasmania. The proxies revealed three broad periods: (1) an early Holocene (11.5–8.3 cal kyr BP) characterised by generally high rainfall, the occurrence of irregular fires, and elevated charcoal influx at 11.4 and 10.2 cal ka BP – conditions compatible with attenuated SWW flow over the site; (2) an ambiguous mid-Holocene (8.3–5 cal kyr BP) that marks the transition from a SWW- to ENSO-dominated climate; and (3) a relatively dry and stable late Holocene (5 cal kyr BP to present) that is consistent with the onset of a climate controlled by ENSO activity (i.e., characterised by a more mean El Niño climate state). The proxy record of Lake Dobson highlights the teleconnections between the equatorial Pacific and southern Australasia.

1. Introduction

The El Niño-Southern Oscillation (ENSO) and Southern Westerly Winds (SWW) are important controls of climate south of the equator. ENSO exerts particularly strong amplitude signatures over the equatorial Pacific Ocean and adjoining landmasses, producing trans-Pacific Ocean oscillations in sea-surface temperature (SST) and sea-level pressure (SLP). Climate anomalies resulting from ENSO activity propagate into the sub- and extra-tropical regions of both hemispheres, where high latitude climate drivers, such as the SWW, play an important role in modulating climate (Hill et al., 2009; Meneghini et al., 2007).

The SWW dominate the climate of the extra-tropics where, unlike in the Northern Hemisphere, large tracts of open ocean permit accelerated wind speeds below the 30th parallel. The extra-tropics are marked by zonally symmetric wind circulation (Garreaud, 2007) that is a key driver of Southern Ocean circulation and productivity, meridional heat transport, deep-water formation, global atmospheric CO_2 levels, and terrestrial climate (Anderson et al., 2009; Garreaud, 2007; Moreno et al., 2010; Toggweiler, 2009; Toggweiler et al., 2006). Recent syntheses of paleoenvironmental data from extra-tropical regions of Australia, New Zealand, and Southern South America (SSA) reveal substantial changes in both the influence of tropical ENSO activity and the position and strength of the SWW during the postglacial period (see Fletcher and Moreno, 2011, 2012; Lamy et al., 2010; McGlone et al., 1993; Shulmeister et al., 2004).

* Corresponding author. School of Geography, Environment and Earth Sciences, Victoria University of Wellington, Wellington 6012, New Zealand.
E-mail addresses: andrew.rees@vuw.ac.nz (A.B.H. Rees), cwynar@unb.ca (L.C. Cwynar), msfl@unimelb.edu.au (M.-S. Fletcher).

http://dx.doi.org/10.1016/j.quascirev.2015.08.022
0277-3791/

Evidence indicates that changes in the position and strength of the SWW drove precipitation patterns throughout the postglacial period, resulting in vegetation and fire-regime changes that appear to be temporally synchronous and zonally symmetric prior to about 5 cal ka BP (Fletcher and Moreno, 2011, 2012). A marked increase in the frequency and intensity of El Niño-rainfall induced debris flows into Laguna Pallcacocha, located in the eastern equatorial Pacific (Moy et al., 2002), corresponds to an apparent breakdown of this zonal symmetry after 5 cal ka BP. Fletcher and Moreno (2012) postulated that an intensification of ENSO after 5 cal ka BP disrupted the previous zonal symmetry driven by the SWW. Indeed, many terrestrial records support an intensification of ENSO-type conditions across the south Pacific sector after ca. 5 cal ka BP, for example: Donders et al. (2007), Lynch et al. (2007), Marx et al. (2009), Quigley et al. (2010), and Shulmeister and Lees (1995) for Australia; Gomez et al. (2011), Hellstrom et al. (1998), and McGlone and Wilmshurst (1999) for New Zealand; and Conroy et al. (2008), Rodbell et al. (1999), and Sandweiss et al. (1996) for South America. While many records report the effects of an intensified ENSO system across the Pacific sector after ca. 5 cal ka BP, few explicitly test the notion that this intensification disrupted extra-tropical SWW climatic dominance. Therefore, the aim of our study is to both determine if and when ENSO began to influence zonal SSW circulation.

Here, we reconstruct postglacial precipitation changes from Lake Dobson, south-central Tasmania (42°S), Australia (Fig. 1). Precipitation at the site is primarily derived from orographic rainfall as the SWW pass over the ranges that bisect Tasmania into wet western and drier eastern sectors, with some incursion of easterly sourced precipitation under reduced SWW flow. Precipitation anomalies in Tasmania are significantly correlated to both ENSO and the Southern Annular Mode (SAM) – an index that describes latitudinal shifts of the SWW (Hendon et al., 2007; Hill et al., 2009; Meneghini et al., 2007). ENSO events exhibit an almost island-wide effect on Tasmania, with El Niño (La Niña) causing anomalously dry (wet) conditions (Hill et al., 2009). Further, in southeast Tasmania, years of extreme negative Southern Oscillation Index values, typical of El Niño episodes, result in more days of both low minimum relative humidity and high Forest Fire Danger Index (FFDI) values (Williams and Karoly, 1999).

The relationship between precipitation and SAM is more spatially constrained. Positive SAM phases correspond to poleward shifts of the SWW core (located at ca. 50°S), reducing rainfall in southern and western Tasmania and having little to no effect in the east. However, when the positive phase of SAM coincides with austral summer, contraction of the SWW is exacerbated, permitting anomalously strong easterly flow at 40°S (Hendon et al., 2007). This configuration again creates below average precipitation in western Tasmania, but above average precipitation in the east (Hill et al., 2009). Negative SAM years result in the opposite effect – the northern margin of the SWW expands across Tasmania, causing anomalously wet conditions in the west and dry conditions in the

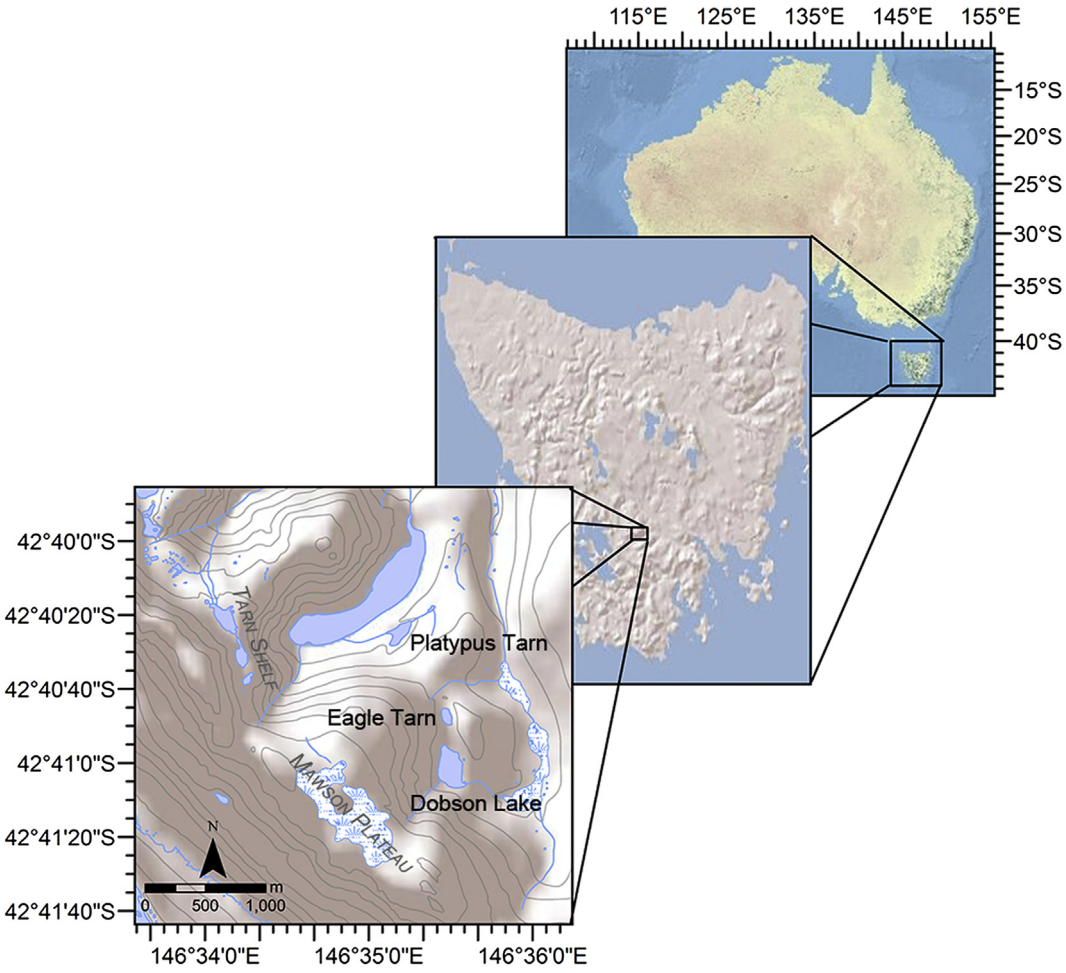

Fig. 1. Study site with proximity of Lake Dobson to the Tarn Shelf, Mawson Plateau, Eagle Tarn, and Platypus Tarn.

east. Lake Dobson is positioned within the transitional zone between the hyper-humid western and the sub-humid eastern regions of Tasmania. By focussing our analysis in this transitional zone, we hope to characterise the dynamic interplay between the SWW and ENSO through time, with a particular focus on the hypothesized 5 cal ka BP juncture. We use chironomids, charcoal, and geochemistry as proxies for various processes related to precipitation, namely stream discharge, lake depth, catchment erosion, and fire-conducive weather.

2. Study area

Lake Dobson (42°41.019′S, 146°35.478′E, surface area 5.6 ha, 1030 m a.s.l.) is a moraine-bound cirque lake located in Mount Field National Park, south-central Tasmania (Fig. 1). The lake is oligotrophic, with light penetrating to 4.1 m, and possesses a simple basin with a broad littoral bench (<3 m) that narrows into a 5.7-m deep cone. The lake's catchment is roughly 91.6 ha and largely falls within a cirque depression. Lake Dobson has one out-flowing and two in-flowing streams; outflow is determined by a sill of glacial till that has scarcely been eroded, while the main in-flow originates from the adjacent Mawson Plateau, roughly 240 m higher in elevation, and drains the cirque headwall. The lake is situated within the subalpine zone of Mount Field and is vegetated by *Eucalyptus* woodland with a shrub understory. Lake Dobson receives about 1650 mm of precipitation annually (475 mm and 310 mm during the wettest and driest quarters, respectively) and has mean temperatures ranging from 1.7 °C during the coldest to 9.5 °C during the warmest quarters. These values were estimated with BIOCLIM − software that combines data from meteorological stations and a digital elevation model to generate point-values for specific climate parameters (Houlder et al., 2003).

The catchment is primarily composed of intrusive Jurassic dolerite, which weathers into krasnozem soils with co-dominant peat (Kidd and Spanswick, 2000). This type of soil is a red podzol formed at an advanced stage of weathering and leaching, rich in the clay mineral kaolinite, with either the iron-containing minerals hematite or goethite, and small amounts of degraded chlorite and quartz (Tiller, 1963). The north-western to south-western aspect of the catchment is particularly steep-sloped, facilitating the delivery of erosional by-products into the basin.

3. Methods

3.1. Sediment retrieval and dating

We retrieved a 1047-cm long sediment core from Lake Dobson during January of 2009 using a modified Livingstone piston corer (Wright et al., 1984); the uppermost, flocculent sediment was collected with a plastic tube fitted with a piston and attached to coring rods (Wright, 1991). Ten terrestrial plant macrofossil samples were collected for AMS ^{14}C dating and submitted to the UCI Keck Carbon Cycle AMS Program at the University of California, Irvine (Table 1). Radiocarbon dates were calibrated with SHCal13 (Hogg et al., 2013), and an age–depth model was developed in R v3.1.2 (R Core Team, 2014) using clam v2.2 (Blaauw, 2010); a smooth spline with a span of 0.1 produced the best goodness-of-fit (Fig. 2). Ages from previous literature reported in radiocarbon years were calibrated to point estimates with OxCal v4.2 (Bronk Ramsey, 2009) using the median of the probability distribution.

Small, open lakes, like Lake Dobson, with perennial water supplies and steep basins provide an ideal setting for recording sediment transport caused by precipitation (Page et al., 1994). During periods of intense rainfall, increased stream velocity and discharge entrain coarse-grained sediment from upland regions, while a steep-sloped catchment facilitates surface runoff. We targeted a suite of biological and geomorphological proxies that reflect these processes.

3.2. Chironomids

Rees et al. (2008) identified annual precipitation as the 5th most important variable structuring the modern distribution of chironomids in Tasmania, explaining 5.6% of the variance in the species data. Of the 49 non-rare taxa surveyed, 19 were significantly ($p \leq 0.05$) related to annual precipitation, with 11 possessing positive and eight possessing negative relationships. The autecology of taxa with positive relationships to high precipitation comprises genera associated with deep lakes, lotic environments, and semi-terrestrial conditions (see Suppl. Fig. 1 for details). We developed a qualitative index of rainfall by calculating the ratio of fossil taxa significantly related to high precipitation environments in the modern training set (Rees et al., 2008) against those significantly related to low precipitation; higher values of the ratio indicate more rainfall.

We collected chironomid samples at 10-cm intervals, with increased resolution for periods of interest, and processed those samples following standard procedures (Walker et al., 1991). An average of 1.4 cm^3 (range: 0.5–5 cm^3) of wet sediment was deflocculated with warm 5% KOH for 20 min and then washed through a nylon sieve with 95-μm meshes. Head capsules were picked, using fine forceps, from a Borgorov tray under 40× magnification and then mounted on slides with Entellan®. Identification was conducted with a compound microscope at 400× magnification following Brooks et al. (2007), Cranston (2010), and Wiederholm (1983). The chironomid stratigraphy was zoned with psimpoll using optimal-splitting by information content, whereby the statistical validity of zones is established by comparison to a broken stick model (Bennett, 2005).

3.3. Geochemistry and grain-size

To complement the chironomid rainfall index, we examined geomorphological proxies that reflect erosional processes occurring within Lake Dobson's catchment. Dolerite, the main parent material in the catchment, is an igneous rock that is primarily composed of silicate minerals, namely plagioclase feldspars, clinopyroxene, and quartz, resulting in a chemistry dominated by silica-, aluminium-, calcium,- and iron-oxides. While quartz is relatively resilient, clinopyroxene, and to a lesser extent plagioclase, weather into clay minerals: kaolinite and smectite (Osok and Doyle, 2004). In high erosional environments, rocks and minerals have shorter catchment residence times before being deposited into lake sediments and, therefore, less time to weather; this setting would produce larger grains. In stable environments, on the other hand, rocks and minerals would have longer residence times in the catchment, so feldspars and pyroxenes would weather into clays. We collected Itrax (μ-XRF) and grain size data to estimate these processes.

We had μ-XRF performed at L'Institut national de la recherche scientifique (INRS), Québec City, using a 2-mm sampling resolution and 20-s exposure time. We expressed results as elements/kcps (thousand counts per spectrum) to account for instrumental bias and the matrix effect (Cuven et al., 2010). We also calculated the Compton/Raleigh scattering (inc/coh), which varies with sediment packing, water volume, and organic content (Croudace et al., 2006). A principal components analysis (PCA), scaled to unit variance, was performed on the major elements.

Table 1
Radiometric dates from Dobson Lake, Mount Field National Park, Tasmania submitted to UCI Keck Carbon Cycle AMS Program at the University of California, Irvine, USA. Calibrations were made in clam v2.2 (Blaauw, 2010) using SHCal13 (Hogg et al., 2013).

UCIAMS no.	Sample depths (cm)	Sample description	^{14}C age (a BP)	95% C.I.[a] (min)	95% C.I.[a] (max)	HPD[b]
76880	116.7–118.7	Leaf & wood fragments	955 ± 20	745	905	95.0
76881	204.9–206.9	Leaf fragments	1795 ± 20	1595	1601	2.0
				1606	1715	92.9
76882	284.4–286.0	Leaf fragments	2555 ± 20	2490	2604	52.0
				2606	2643	15.5
				2653	2668	2.3
				2676	2739	25.2
76883	392.2–394.2	Leaf fragments, stems	3750 ± 25	3932	3941	1.5
				3969	4104	79.1
				4106	4149	14.3
76884	529.0–531.0	Wood fragments	5790 ± 20	6468	6638	95.0
76885	598.0–600.0	Wood fragments	8235 ± 25	9029	9259	95.0
76886	695.8–697.8	Leaf & wood fragments	9795 ± 35	11,110	11,111	0.3
				11,122	11,242	94.6
76887	777.1–782.1	Leaf & wood fragments	12,035 ± 35	13,741	13,988	95.0
76888	824.0–826.0	Leaf & wood fragments	12,240 ± 30	13,969	14,210	95.0
76889	927.0–928.0	Leaf & wood fragments	12,555 ± 35	14,406	15,079	95.0

[a] C.I. = Confidence interval.
[b] HPD = Highest probability density.

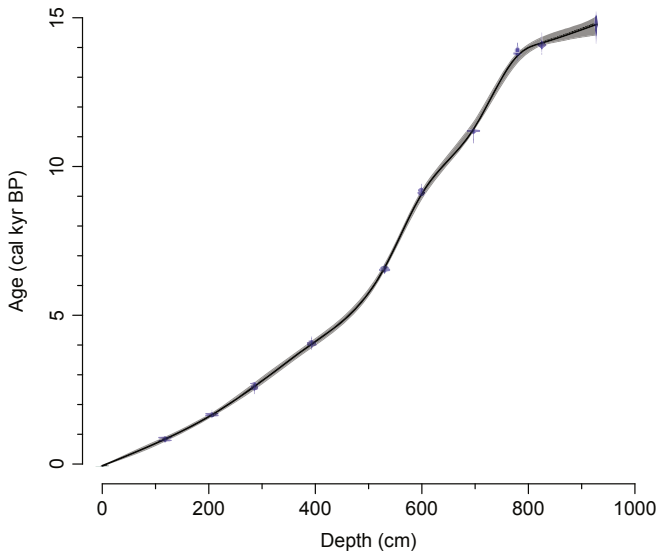

Fig. 2. Age–depth model for Lake Dobson derived from 10 terrestrial macrofossils. The age–depth model was developed in clam v2.2 (Blaauw, 2010) using SHCal13 (Hogg et al., 2013). Blue bars represent the highest probability density of each date, while the grey fill displays the 95% confidence intervals of the calibration range. Average accumulation is 4.2, 3.7, and 9.2 cm/century for the early, mid-, and late Holocene, respectively. (For interpretation of the references to colour in this figure legend, the reader is referred to the web version of this article.)

We analysed grain size samples using Geological Survey of Canada, Atlantic (GSCA), standard protocol. Grain sizes were measured every 10 cm on wet sediment placed into a 50-mL conical base centrifuge tube (filled to approximately the 5-mL mark). Samples were prepared for grain size analysis by digestion using 35% hydrogen peroxide for 24 h at room temperature and for an additional 8 h at 60 °C. Following digestion, samples were centrifuged, decanted, and freeze-dried. A portion of well-mixed sediment was further disaggregated using an ultrasonic bath for 15 s before being completely introduced into the Beckman Coulter LS230 laser diffraction unit at the Bedford Institute of Oceanography, Halifax. We define grain size classes according to the International Organization for Standardization (ISO), where clay is less than 2 μm, silt is between 2 and 63 μm, and sand is between 63 and 2000 μm.

3.4. Charcoal

Charcoal, a proxy of fire history, was sampled every 1 cm and processed following a protocol developed from methods in Enache and Cumming (2007), Long et al. (1998), and Walsh et al. (2010). Samples of 2 cm^3 (surface core) and 4 cm^3 (long core) were disaggregated in 40 mL of 10% KOH for 24 h, then 40 mL of 6% sodium hypochlorite were added and, after one hour, samples were gently washed through sieves with 250- and 150-μm meshes. The 150–250-μm fraction was washed into a gridded Petri dish, and charcoal fragments were enumerated using a stereoscope at about 17× magnification. The statistical treatment of charcoal data was primarily conducted in CharAnalysis (Higuera et al., 2009), where charcoal influx (CHAR) is decomposed into background ($C_{background}$) and peak (C_{peak}) components, and a locally defined threshold is used to identify charcoal peaks likely related to fires within a 1-km radius of Lake Dobson. The data were then interpolated ($C_{interpolated}$) to the median sample resolution of the record. $C_{background}$ was smoothed using a moving mode set to a 500-year window. C_{peak} was calculated as a residual (i.e. $C_{peak} = C_{interpolated} - C_{background}$) and was assumed to represent two subpopulations: C_{noise}, a component comprising sediment mixing, sampling, and analytical and naturally occurring noise; and C_{fire}, a component representing charcoal derived from actual fires. We used a Gaussian mixture model to determine the distribution of C_{noise} and considered the 99th percentile as a threshold for C_{fire} (i.e. actual fires occurring within 1 km of Lake Dobson). For more details on CharAnalysis, see Higuera et al. (2009).

3.5. Statistical analyses

To summarise the data, we included accumulation rates from clam's age–depth model; the percent abundances of grain size classes (i.e., sand, silt, clay), centred and log ratio-transformed; elemental μ-XRF data normalised to kcps; and CHAR in a PCA, scaled to unit variance. The percent abundances of grain size classes were centred and log ratio-transformed to account for the closure problem associated with compositional data (Aitchison, 1986), while μ-XRF data were fitted to a loess curve to highlight major trends. Further, the accumulation rates, μ-XRF data, and CHAR were linearly interpolated to the resolution of the grain size results, as the latter possessed the coarsest sampling resolution. A broken

stick analysis was performed to identify the appropriate number of principal components (PC) to interpret, and the PCA biplots were colour-coded according to the zones derived from the chironomid stratigraphy. All methods associated with the PCA were implemented in R (R Core Team, 2014).

4. Results

We focus on the portion of Lake Dobson's record postdating the deposition of highly minerogenic sediments, as indicated by the μ-XRF data; this includes the sequence from 11.5 cal ka BP to present. Further, the onset of this part of the record coincides with the establishment of *Nothofagus* forest, evidenced by the pollen record from adjacent Eagle Tarn (Macphail, 1979). The broken stick analysis identifies three zones within the chironomid stratigraphy, here informally referred to as the early (11.5–8.3 cal kyr BP), mid- (8.3–5 cal kyr BP), and late (5 cal kyr BP to present) Holocene.

4.1. Early Holocene (11.5–8.3 cal kyr BP)

The chironomid assemblage of the early Holocene is dominated by *Chironomus* and *Tanytarsus* morphotypes 2 and 3 (Fig. 3). Taxa preferring high precipitation environments are all present at or near peak abundance. The corresponding precipitation index has troughs at 11.4 and 10.2 cal ka BP and peaks at 10.6 and 9.5 cal ka BP (Fig. 4f).

The average sedimentation rate at Lake Dobson is 4.2 cm/century during the early Holocene (Figs. 2 and 5). These sediments possess the largest median grain sizes, 51 μm on average, and consist of 21, 66, and 13% sand, silt, and clay, respectively; the sand fraction contains the highest frequency of particles >500 μm for the entire record (Fig. 4c–e). The major elements are all generally above average. Nickel (Ni), copper (Cu), and zinc (Zn) increase during this phase, with peak values around 9.5 cal ka BP (Fig. 5).

CharAnalysis identifies 15 local fires during the early Holocene, generating a return interval of 213 years. Average CHAR is 4.7 pieces cm^{-2} yr^{-1}, with maxima at 11.4 and 10.2 cal ka BP (Fig. 4h).

4.2. Mid-Holocene (8.3–5 cal kyr BP)

At the onset of the mid-Holocene, *Chironomus* decreases from an average of 35%–5% abundance, and *Parochlus* nearly disappears from this portion of the record entirely. Several taxa preferring low precipitation environments increase during this phase, though *Tanytarsus* morphotype 2 remains dominant during the mid-Holocene (Fig. 3). The precipitation index is generally low, with the exception of slightly elevated values between 7.5 and 6.5 cal kyr BP (Fig. 4f).

Accumulation is lower during the mid-Holocene, averaging 3.7 cm/century; however the trend increases throughout this phase (Figs. 2 and 5). Median grain size decreases to an average of 38 μm, comprised of 16% sand, 72% silt, and 12% clay; the occurrences of grains >500 μm are less frequent (Fig. 4c–e). Many of the major elements are elevated between 7.3 and 6.3 cal kyr BP (Fig. 5).

The mid-Holocene sediments of Lake Dobson archive 14 fires, producing a return interval of 237 years. Average CHAR decreases to 2.9 pieces cm^{-2} yr^{-1}, with a generally increasing trend from a minimum around 8.3 cal ka BP toward the onset of the late Holocene (Fig. 4h).

4.3. Late Holocene (5000 cal kyr BP to present)

The chironomid community of the late Holocene is highly variable. Taxa preferring both high and low precipitation environments occur in abundance. The precipitation index is low throughout this phase, with minor excursions at 3.4 cal ka BP and between 1.5 and 0.5 cal kyr BP (Fig. 4f).

The average accumulation rate increases to 9.2 cm/century during the late Holocene (Figs. 2 and 5). This is accompanied by a reduction in average median grain size to 30 μm, consisting of 13, 72, and 15% average sand, silt, and clay, respectively; grains >500 μm disappear at 5 cal ka BP and return around present (Fig. 4c–e). Detrital indicators like calcium (Ca), iron (Fe), and titanium (Ti) are all generally below average, with frequent and irregular positive excursions (Fig. 5).

CharAnalysis identifies 35 fires during the late Holocene, producing a return interval of 145 years. CHAR averaged 6.1 pieces cm^{-2} $year^{-1}$, with elevated values throughout the late Holocene and a distinct increase over the last 0.5 cal ka BP (Fig. 4h).

5. Discussion

Our multi-proxy analysis provides a detailed reconstruction of the climatic and environmental history of Lake Dobson, a site located within the mid-latitudes of the Southern Hemisphere. The lake lies in a zone sensitive to shifts in the SWW and precipitation anomalies, contributing hydroclimate proxy data necessary for testing hemispheric-scale climate models. Our results reveal millennial to sub-millennial hydrological variation in a region where there is an urgent need for long-term, high-resolution, and precisely dated climate proxy records. Regarding our objectives, we identify the transition from a SWW- to ENSO-dominated climate,

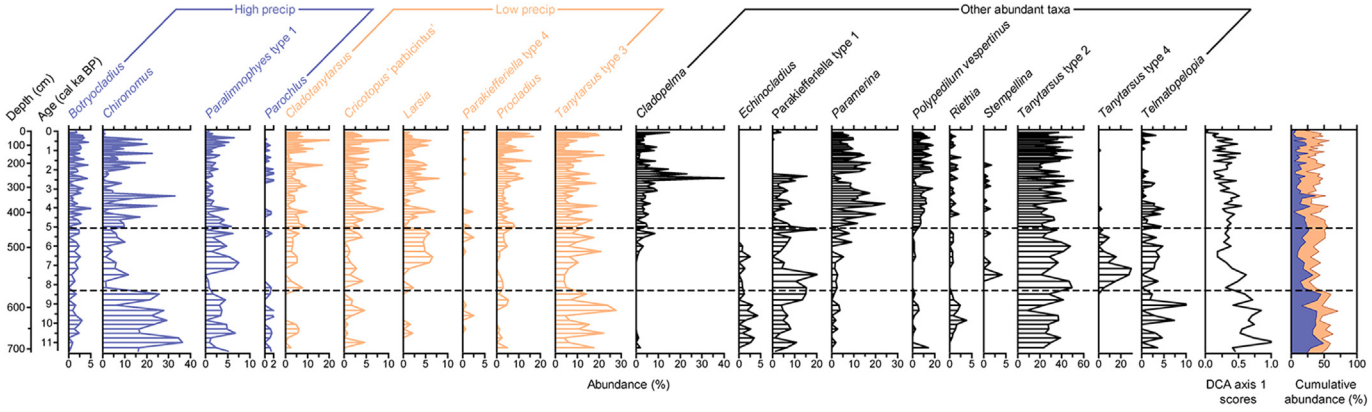

Fig. 3. Chironomid stratigraphy of Lake Dobson with taxa that prefer high and low precipitation environments and other abundant taxa. DCA axis 1 scores estimate species turnover.

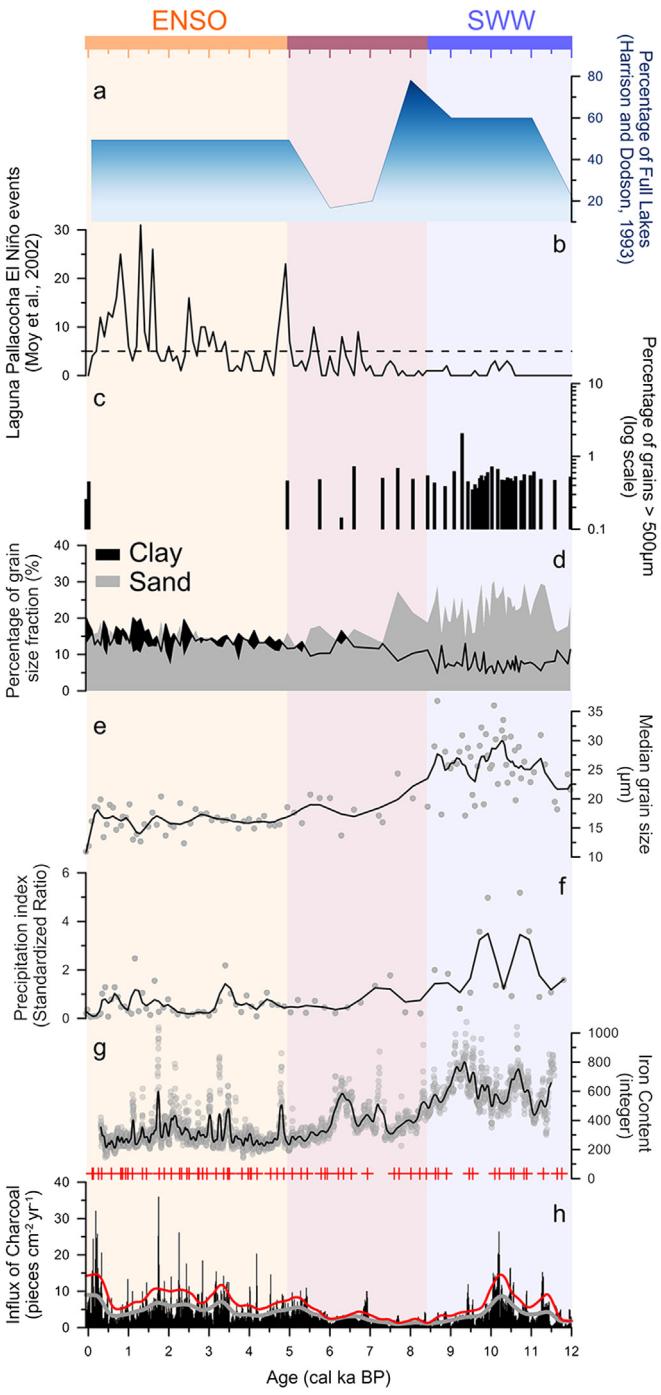

Fig. 4. Summary figure including a) the percentage of full lakes in eastern and central Tasmania (Harrison and Dodson, 1993) and b) the number of El Niño events at Laguna Pallcacocha, Ecuador, in 100-year overlapping windows (Moy et al., 2002). The figure also includes the suite of lacustrine proxies from Lake Dobson, namely: c) the percentage of grains larger than 500 µm (note the log scale), d) the percentage of sand and clay constituting each sample and e) the median grain size of the sediment; f) the precipitation index calculated from fossil chironomid taxa; g) PCA axis 1 scores derived from the geochemical data; and h) charcoal influx rates with background levels (grey line), threshold limits (red line), and fires (red plus symbols). The dashed line in b denotes the minimum number of events needed to produce an ENSO band. Solid black lines in the e, f, and g represent running averages. Colour coding reflects zones identified from the chironomid stratigraphy. (For interpretation of the references to colour in this figure legend, the reader is referred to the web version of this article.)

which was completed by 5 cal ka BP. Lake Dobson archives three distinct phases throughout the Holocene: an early Holocene when SWW dominate, with clear sub-millennial climate oscillations; an ambiguous mid-Holocene transitional phase between SWW dominance and increased ENSO influence; and a late Holocene phase where climate trends are controlled by ENSO variability.

5.1. Early Holocene – SWW dominance

The period of SWW dominance at Lake Dobson comprises the early Holocene, from 11.5 to 8.3 cal kyr BP, and we suggest that synoptic climate around Tasmania was analogously configured to the positive phase of SAM during the summer. In this configuration, the SWW are contracted furthest to the south, and anomalous easterlies develop at 40°S (Hendon et al., 2007). Reduced westerlies promote dry conditions in western Tasmania, and moisture bearing easterlies would enhance both precipitation and detrital input at Lake Dobson.

Trends in the detrital indicators closely match high precipitation inferred from the chironomid record at Lake Dobson. The large grain sizes comprising these sediments suggest short residence times of minerals in the catchment before deposition into the lake (Gabet, 2007; Norton and Blanckenburg, 2010). Trends in potassium (K), Ca, Fe, and manganese (Mn) generally follow Ti, a lithogenic element considered geochemically stable (Boës et al., 2011), implying increased erosion of detrital material (feldspars and pyroxenes) into the lake (Figs. 5 and 6). Above average Fe and Mn, elements sensitive to redox conditions (Davison, 1993; Francus et al., 2013), likely reflect anaerobiosis, reducing conditions that mobilise and leach Fe and Mn from the soil system, indicating that catchment soils were intermittently waterlogged. The increase of Ni, Cu, and Zn at 9.5 cal ka BP corresponds to a drop in the precipitation index (Fig. 4); a decrease in the frequency of the largest grain sizes; and increased autochthonous productivity, highlighted by the increasing inc/coh ratio (Figs. 5 and 6). These elements readily complex with organic ligands (Tyler and McBride, 1982), precipitating from the water column into the lake sediment and imply that erosion was still pronounced after 9.5 cal ka BP; however, conditions were stable enough to promote within-lake productivity.

The SWW dominant period possesses the highest abundance of taxa preferring wet environments and the lowest abundance of taxa preferring dry environments (Fig. 3). Critically *Parochlus*, a taxon that inhabits cool springs and running waters (Brundin, 1983), is present throughout this portion of the record, suggesting appreciable stream discharge from the Mawson Plateau. Low chironomid-inferred precipitation phases at 11.4 and 10.2 cal ka BP are coeval with minima in the detrital indicators and increased charcoal input, while decreased charcoal influx occurs when precipitation and detrital input are high, at ca. 10.6 and 9.5 cal ka BP. These relationships suggest that periods of low rainfall coincide with decreased erosion and increased catchment burning and vice versa. Fires in cool-temperate Tasmania are climate-limited, supporting this inference.

Evidence from other Tasmanian sites corroborates this climate configuration. At adjacent Eagle Tarn, the shift from a *Eucalyptus–Phyllocladus* association to a *Nothofagus* rainforest, occurring ca. 11.5 cal ka BP (9960 ± 300 ^{14}C a BP, Macphail, 1979), suggests the surrounding area became cooler and wetter at the onset of the Holocene, consistent with the chironomid-based temperature estimates from Mount Field (Rees and Cwynar, 2010) and the inferred wet phase presented here. Increased rainfall also corresponds to a period of lake high-stands in eastern Tasmania (Fig. 4a; Harrison and Dodson, 1993). Meanwhile, a positive SAM and weak SWW circulation would also tend towards drier conditions in western Tasmania (Hendon et al., 2007; Hill et al., 2009), as postulated by Fletcher and Moreno (2012). Using a composite charcoal profile for western Tasmania and a paleovegetation index

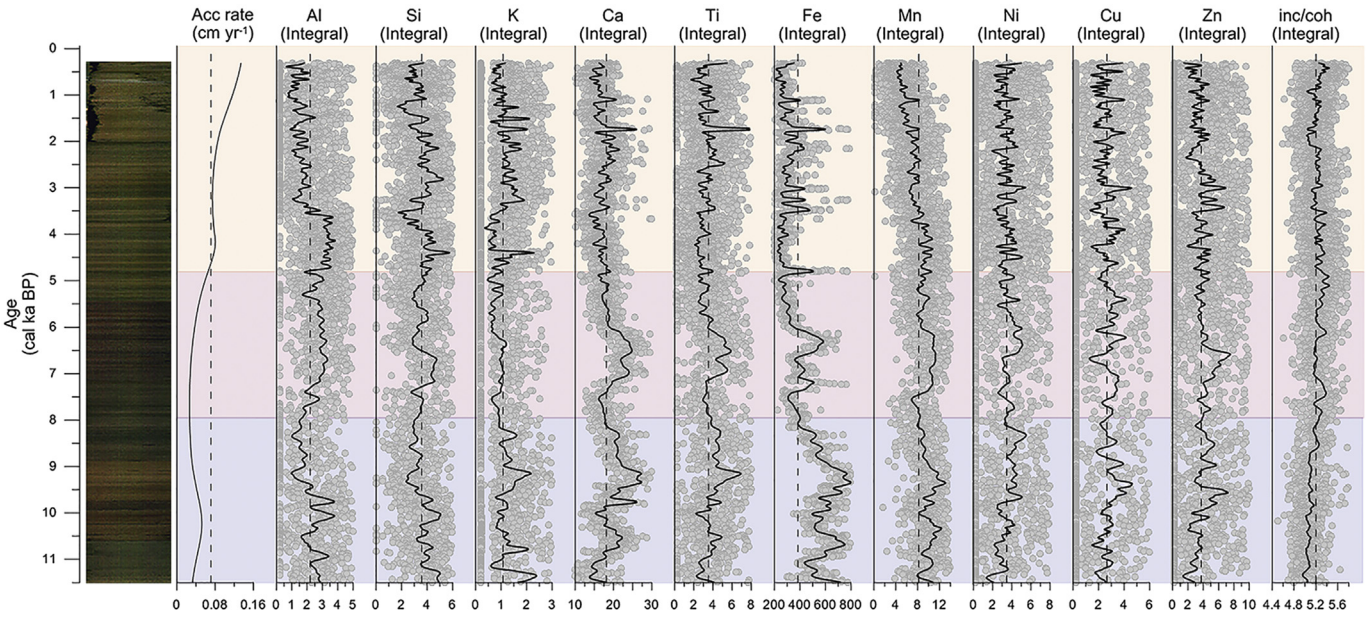

Fig. 5. Stratigraphical sequence of the Lake Dobson sediment record along with trends in major elements. All elemental values have been normalised to thousand counts per spectrum (kcps) to account for the matrix effect. The inc/coh ratio is related to the sediment packing, water volume, and organic content (Croudace et al., 2006).

developed from the Lake Vera pollen record, those authors argued for drier conditions in western Tasmania from 11 to 8 kyr BP driven by a zonally symmetric decrease in SWW flow. Further, many have argued for weakened SWW circulation during the early Holocene from records throughout the Southern Hemisphere (e.g. Fletcher and Moreno, 2012; Kilian and Lamy, 2012; Markgraf et al., 2007; Moreno et al., 2010; Moy et al., 2011; Whitlock et al., 2007).

5.2. Mid-Holocene – transitional period

The mid-Holocene, from 8.3 to 5 cal ka BP, demarks the transitional period from SWW dominance to enhanced ENSO influence. Both the large grain sizes and abundant detrital content of the SWW dominant period shift to finer sediments with a higher organic content, characterising the period of pronounced ENSO activity (Figs. 4 and 5). While fewer large grains and decreasing grain sizes and precipitation index values support stable, dry conditions transitioning into the late Holocene, the detrital indicators are elevated between 7.3 and 6.3 cal kyr BP and coincide with infrequent fires, suggesting enhanced precipitation.

Evidence from other Tasmanian sites supports either case. Reversion from *Nothofagus* rainforest to a *Phyllocladus–Eucalyptus* association at Eagle Tarn suggests conditions may have become drier (Macphail, 1979); this is consistent with a low percentage of full lakes in eastern Tasmania (Fig. 4a; Harrison and Dodson, 1993). At Lake Vera, above average precipitation was inferred between 7 and 5 cal ka BP from lithostratigraphy, palynology, and charcoal evidence (Fletcher and Moreno, 2012). Indeed, several studies show continuously increasing strength of the SWW starting in the middle Holocene (Fletcher and Moreno, 2012; Gilli et al., 2005; Moreno et al., 2010; Moy et al., 2011). Strengthened westerlies would deliver precipitation to western Tasmania; however, foehn winds would both increase evaporation and prevent the incursion of moisture bearing easterlies, resulting in dryness in the east (Fletcher and Moreno, 2012). Contrary to this evidence, a speleothem record from northern Tasmania supports elevated precipitation during the mid-Holocene (Xia et al., 2001).

Based on growth rates and $^{234}U/^{238}U$ ratios measured on a speleothem at Lynd's Cave, Xia et al. (2001) inferred reduced effective precipitation between 8 and 7.4 kyr BP followed by a sharp increase between 7.4 and 7 kyr BP. Precipitation then declined between 7 and 6.6 kyr BP before significant climatic deterioration between 6.6 and 5.1 kyr BP. This generally matches trends in the detrital indicators from Lake Dobson's sedimentary record (Fig. 5), suggesting that the transition to the period of more frequent El Niño events may be more complex than implied by the grain size data and precipitation index.

5.3. Late Holocene – ENSO dominance

The best evidence for the onset of an ENSO-dominated climate during the late Holocene at Lake Dobson is the elevated $C_{background}$ and short fire return intervals, coinciding with more frequent El Niño events recorded by the classic record from Laguna Pallcacocha, Ecuador (Fig. 4b and h; Moy et al., 2002). Bushfires in Tasmania have been linked to strongly negative SOI values (Grose et al., 2014; Nicholls and Lucas, 2007; Williams and Karoly, 1999).

However, the relationship between climate, fire, and catchment geomorphology is complex. More charcoal does not equate to more fire and, as evidenced at Lake Osborne in southwest Tasmania, fire events do not necessarily elicit catchment responses (Fletcher et al., 2013). This is perhaps best exemplified by the short CHAR vector length with respect to PC1 and PC3; further, that vector is nearly orthogonal to or oriented in the opposite direction of the detrital indicators Fe, Ca, and Ti (Fig. 6), suggesting no or inverse relationships, respectively. These features highlight both the non-linear association between fire and landscape dynamics and the variable nature of ENSO's expression in the mid-latitudes of the Southern Hemisphere. Further, the fact that elevated background burning counterintuitively does not elicit a catchment response in the grain size data suggests that Lake Dobson may archive a regional, rather than local, fire history. What can be concluded is, at the millennial scale, a more mean El Niño climate-state at Laguna Pallcacocha corresponds to a shortened fire return interval and increased background burning in Tasmania, highlighting teleconnections to the equatorial Pacific, although attributing drivers to

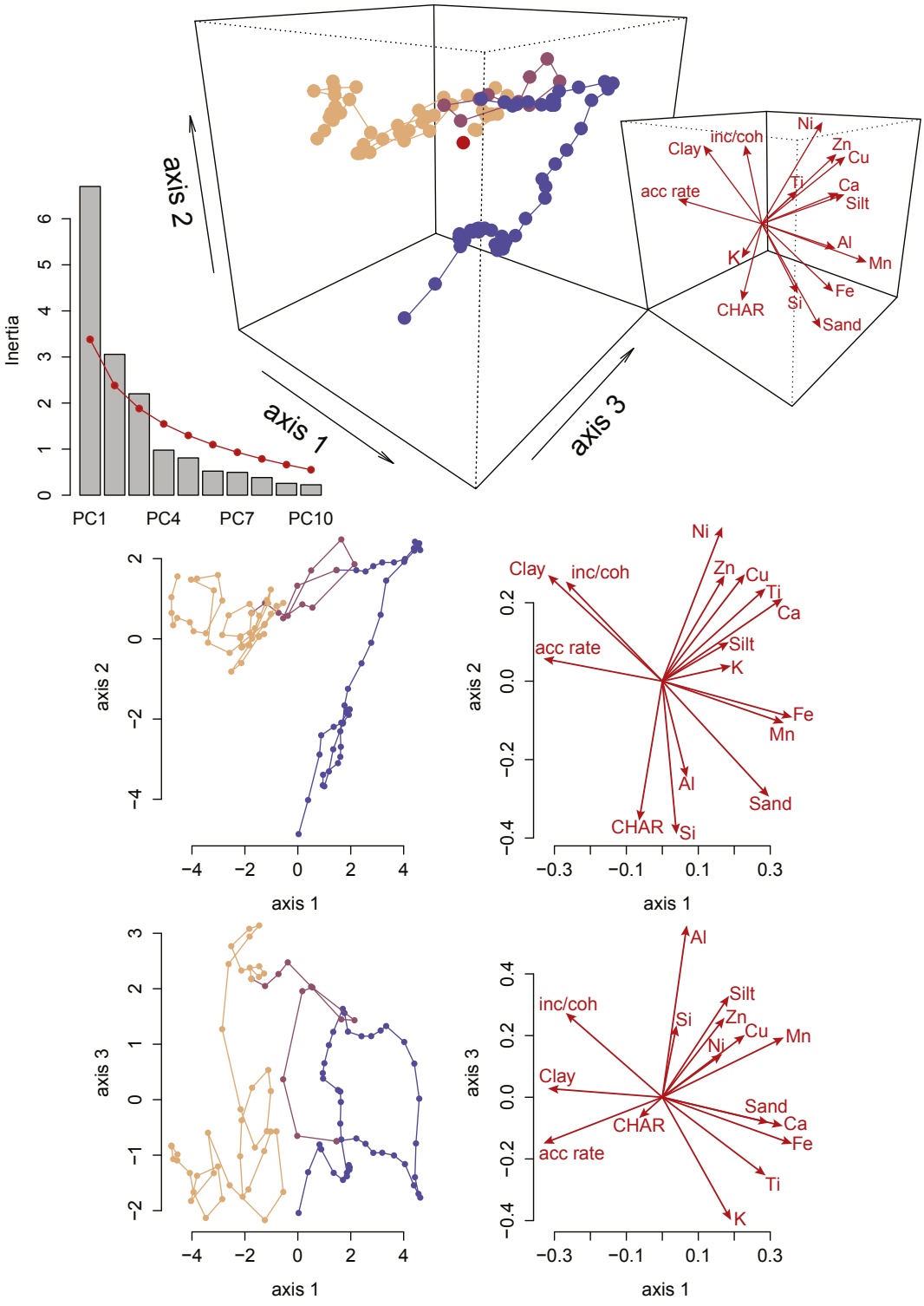

Fig. 6. PCA of the μ-XRF data, grain size classes, and CHAR; sample scores are coloured according to the zonation of the chironomid stratigraphy. A broken stick analysis identified the first three principal components (PC) as significant. PC1, PC2, and PC3 explain 42, 19, and 14% of the variance, respectively.

sub-millennial events remains difficult.

Underlying the short fire return interval and increased $C_{background}$ are the smallest median grain sizes for the entire record. Clay and sand appear in equal parts and the largest grain size class almost completely disappears. Together with the precipitation index and below-average values for the majority of major elements, these proxies suggest that erosional processes requiring high-energy inputs were diminished. Considering the elevated accumulation rates and inc/coh ratio characterising the late Holocene (Figs. 5 and 6), within-lake productivity must have increased. In short, all proxies suggest that Lake Dobson's catchment was relatively stable and dry.

Currently, anomalously dry years are associated with a high pressure cell over Tasmania, which drives calm, stable weather (Hill et al., 2009). ENSO cycles exhibit an island-wide effect on Tasmania, with El Niño (La Niña) causing anomalously dry (wet) years (Hill et al., 2009). The leading empirical orthogonal function (EOF), calculated on rainfall climatology for the period between 1950 and 2005, explained 72% of the variance in the 55-year data set. The EOF was primarily related to ENSO, the Pacific-South American mode (PSA) and, to a lesser extent, SAM (Hill et al., 2009). Extrapolating this pattern back to the onset of enhanced El Niño activity around 5 cal ka BP (Fig. 4b; Moy et al., 2002), and considering proxy relationships established during the SWW dominant period, we would expect an increased fire frequency, less erosion, and generally lower values for the precipitation index during El Niño phases; the Lake Dobson proxies demonstrate this pattern.

Vegetation development at Eagle Tarn further supports this notion of relatively dry and stable conditions. *Eucalyptus* becomes increasingly dominant throughout the late Holocene, first occurring with *Phyllocladus* and *Microstrobos*, and then with *Microstrobos* and a minor component of *Lagarostrobos* (Macphail, 1979). At Lake Osborne, sequential fires from 6.5 cal ka BP to present resulted in the replacement of pyrophobic rainforest with pyrogenic *Eucalyptus*-dominated vegetation (Fletcher et al., 2013). Wet sclerophyll *Eucalyptus* forests are better adapted to surviving short fire return intervals (Fletcher et al., 2014), which characterise Lake Dobson's late Holocene. However, the persistence of *Microstrobos* and *Lagarostrobos*, pyrophobic taxa preferring cool and moist conditions, in the Eagle Tarn pollen record suggests sufficient moisture at Mount Field to maintain this heterogeneous mosaic of vegetation, which is consistent with the reappearance of *Parochlus* during the late Holocene (Fig. 3).

Currently, a significant body of evidence purports that the frequency of El Niño events increased at about 5 cal ka BP, and the resultant effects were manifest throughout many of the landmasses occupying the Southern Hemisphere (see references in the Introduction). The breakdown from a generally wet early Holocene to a variable though dry late Holocene was clearly captured by the proxy record archived in Lake Dobson, which responded in concert with climatological events originating in the equatorial Pacific. At the millennial scale, a more mean El Niño state corresponds to greater background charcoal influx at Lake Dobson.

6. Conclusions

Lake Dobson lies within a critical region of the Southern Hemisphere's mid-latitudes, affording the unique opportunity to reconstruct the dynamic interplay between the SWW and ENSO. ENSO influence became established at Lake Dobson at 5 cal ka BP, after a 3.3 kyr transitional period that demarked the waning of SWW dominance. During the period when Tasmanian climate was controlled by the SWW, the westerlies were attenuated, locked in a phase similar to a modern positive SAM during the summer. The period between 8.3 and 5 cal kyr BP marked the transition to an ENSO-dominated climate and was either uniformly dry or generally dry, though punctuated by elevated precipitation between 7.3 and 6.3 cal kyr BP. The interval of more mean El Niño-like conditions at Lake Pallcacocha, starting around 5 cal ka BP, closely matches the climatology associated with Lake Dobson's catchment, suggesting a tight link between Tasmania and the equatorial Pacific. From 5 cal kyr BP to present, Lake Dobson archives variable conditions, fluctuating between predominant, dry El Niño phases and intermittent, wet La Niñas. This coincides with the onset of ENSO-induced variability demonstrated both locally and throughout many of the landmasses occupying the Southern Hemisphere.

Acknowledgements

We thank Marian and Rob Wiltshire for their hospitality and support. We also thank Maarten Blaauw for his invaluable help with clam, Owen Brown for assisting with the collection of the grain size data, and Pierre Francus and Ben Hines for consulting with the interpretation of the Itrax results. John Southon provided the radiocarbon dates. We are also grateful to Greg Jordan, Vera Markgraf, and Jamie Shulmeister for providing helpful comments on earlier drafts. Finally, we thank the two anonymous reviewers whose comments made this a stronger manuscript. This research was supported by a Natural Sciences and Engineering Research Council of Canada (NSERC) 39785-2010 Discovery grant to Les C. Cwynar and an NSERC Postgraduate Scholarship to Andrew B.H. Rees.

Appendix A. Supplementary data

Supplementary data related to this article can be found at http://dx.doi.org/10.1016/j.quascirev.2015.08.022.

References

Aitchison, J., 1986. The Statistical Analysis of Compositional Data. Chapman and Hall, London – New York.
Anderson, R.F., Ali, S., Bratmiller, L.I., Nielsen, S.H.H., Fleisher, M.Q., Anderson, B.E., Burkle, L.H., 2009. Wind-driven upwelling in the southern ocean and the deglacial rise in atmospheric CO_2. Science 323, 1443–1448.
Bennett, K.D., 2005. Documentation for Psimpoll 4.25 and Pscomb 1.03: C Programs for Plotting Pollen Diagrams and Analysing Pollen Data. Software Manual. Uppsala Universitet, Uppsala, Sweden.
Blaauw, M., 2010. Methods and code for 'classical' age-modelling of radiocarbon sequences. Quat. Geochronol. 5, 512–518.
Boës, X., Rydberg, J., Martinez-Cortizas, A., Bindler, R., Renberg, I., 2011. Evaluation of conservative lithogenic elements (Ti, Zr, Al, and Rb) to study anthropogenic element enrichments in lake sediments. J. Paleolimnol. 46, 75–87.
Brodin, Y.W., 1986. The postglacial history of Lake Flarken, southern Sweden, interpreted from subfossil insect remains. Intern. Revue Hydrobiol. 71, 371–432.
Bronk Ramsey, C., 2009. Bayesian analysis of radiocarbon dates. Radiocarbon 51, 337–360.
Brooks, S.J., Langdon, P.G., Heiri, O., 2007. Using and Identifying Chironomid Larvae in Palaeoecology. QRA Technical Guide No. 10. Quaternary Research Association, London, UK.
Brundin, L., 1983. The larvae of Podonominae (Diptera: Chironomidae) of the Holarctic region – keys and diagnoses. Entomol. Scand. (Suppl. 19), 23–31.
Conroy, J.L., Overpeck, J.T., Cole, J.E., Shanahan, T.M., Steinitz-Kannan, M., 2008. Holocene changes in eastern tropical Pacific climate inferred from a Galápagos lake sediment record. Quat. Sci. Rev. 27, 1166–1180.
Cranston, P.S., 2010. Chiro Key. Available. http://chirokey.skullisland.info/.
Cranston, P.S., Edward, D.H.D., 1999. *Botryocladius* gen.n.: a new transantarctic genus of orthocladiine midge (Diptera: Chironomidae). Syst. Entomol. 24, 305–333.
Croudace, I.W., Rindby, A., Rothwell, R.G., 2006. ITRAX: description and evaluation of a new multi-function X-ray core scanner. Geol. Soc. Lond. Spec. Publ. 267, 51–63.
Cranston, P.S., Oliver, D.R., Sæther, O.A., 1983. The larvae of the Orthocladiinae (Diptera:Chironomidae) of the Holarctic region - keys and diagnoses. Entomol. Scand. (Suppl. 19), 149–291.
Cuven, S., Francus, P., Lamoureux, S.F., 2010. Estimation of grain size variability with micro X-ray fluorescence in laminated lacustrine sediments, Cape Bounty, Canadian High Arctic. J. Paleolimnol. 44, 803–817.
Davison, W., 1993. Iron and manganese in lakes. Earth Sci. Rev. 34, 119–163.
Donders, T.H., Haberle, S., Hope, G., Wagner, F., Visscher, H., 2007. Pollen evidence for the transition of the eastern Australian climate system from the post-glacial to the present-day ENSO mode. Quat. Sci. Rev. 26, 1621–1637.
Enache, M.D., Cumming, B.F., 2007. Charcoal morphotypes in lake sediments from British Columbia (Canada): an assessment of their utility for the reconstruction of past fire and precipitation. J. Paleolimnol. 38, 347–363.
Fletcher, M.-S., Moreno, P.I., 2011. Zonally symmetric changes in the strength and position of the Southern Westerlies drove atmospheric CO_2 variations over the past 14 ky. Geology 39, 419–422.
Fletcher, M.-S., Moreno, P.I., 2012. Have the Southern Westerlies changed in a zonally symmetric manner over the last 14,000 years? A hemisphere-wide take on a controversial problem. Quat. Int. 253, 32–46.
Fletcher, M.-S., Wood, S.W., Haberle, S.G., 2013. A fire driven shift from forest to non-forest: evidence for alternative stable states? Ecology 95, 2504–2513.
Fletcher, M.-S., Wolfe, B.B., Whitlock, C., Pompeani, D.P., Heijnis, H., Haberle, S.G.,

Gadd, P.S., Bowman, D.M.J.S., 2014. The legacy of mid-Holocene fire on a Tasmanian montane landscape. J. Biogeogr. 41, 476–488.
Francus, P., Von Suchodoletz, H., Dietze, M., Donner, R.V., Bouchard, F., Roy, A.-J., Fagot, M., Vershuren, D., Kröpelin, S., 2013. Varved sediments of Lake Yoa (Ounianga Kebir, Chad) reveal progressive drying of the Sahara during the last 6100 years. Sedimentology 60, 911–934.
Gabet, E., 2007. A theoretical model coupling chemical weathering and physical erosion in landslide-dominated landscapes. Earth Planet. Sci. Lett. 264, 259–265.
Garreaud, R.D., 2007. Precipitation and circulation covariability in the extratropics. J. Clim. 20, 4789–4797.
Gilli, A., Ariztegui, D., Anselmetti, F.S., McKenzie, J.A., Markgraf, V., Hajdas, I., McCulloch, R.D., 2005. Mid-holocene strengthening of the Southern Westerlies in South America – sedimentological evidences from Lago Cardiel, Argentina (49°S). Glob. Planet. Chang. 49, 75–93.
Gomez, B., Carter, L., Orpin, A.R., Cobb, K.M., Page, M.J., Trustrum, N.A., Palmer, A.S., 2011. ENSO/SAM interactions during the middle and late Holocene. Holocene 22, 23–30.
Grose, M.R., Fox-Hughes, P., Harris, R.M.B., Bindoff, N.L., 2014. Changes to the drivers of fire weather with a warming climate – a case study of southeast Tasmania. Clim. Change 124, 255–269.
Harrison, S.P., Dodson, J.R., 1993. Climates of Australia and New Guinea since 18,000 yr B.P. In: Wright Jr., H.E., Kutzbach, J.E., Webb III, T., Ruddiman, W.F., Street-Perrot, F.A., Bartlein, P.J. (Eds.), Global Climates since the Last Glacial Maximum. University of Minnesota Press, Minneapolis, MN, pp. 265–293.
Hellstrom, J., McCulloch, M., Stone, J., 1998. A detailed 31,000-year record of climate and vegetation change, from the isotope geochemistry of two New Zealand speleothems. Quat. Res. 50, 167–178.
Hendon, H.H., Thompson, D.W.J., Wheeler, M.C., 2007. Australian rainfall and surface temperature variations associated with the southern hemisphere annular mode. J. Clim. 20 (11), 2452–2467.
Higuera, P.E., Brubaker, L.B., Anderson, P.M., Hu, F.S., 2009. Vegetation mediated the impacts of postglacial climate change on fire regimes in the south-central Brooks Range, Alaska. Ecol. Monogr. 79, 201–219.
Hill, K.J., Santoso, A., England, M.H., 2009. Interannual Tasmanian rainfall variability associated with large-scale climate modes. J. Clim. 22, 4383–4397.
Hogg, A.G., Hua, Q., Blackwell, P.G., Niu, M., Buck, C.E., Guilderson, T.P., Heaton, T.J., Palmer, J.G., Reimer, P.J., Reimer, R.W., Turney, C.S.M., Zimmerman, S.R.H., 2013. SHCal13 southern hemisphere calibration, 0–50,000 years cal BP. Radiocarbon 55, 1–15.
Houlder, D., Hutchinson, M., Nix, H.A., McMahon, J., 2003. ANUCLIM User's Guide. Australian National University, Canberra, Australia.
Kidd, D., Spanswick, S., 2000. Revised Burnie-table Cape Reconnaissance Soil Map of Tasmania. Department of Primary Industry Water & Environment.
Kilian, R., Lamy, F., 2012. A review of Glacial and Holocene paleoclimate records from southernmost Patagonia (49–55°S). Quat. Sci. Rev. 53, 1–23.
Lamy, F., Kilian, R., Arz, H.W., Francois, J.P., Kaiser, J., Prange, M., Steinke, T., 2010. Holocene changes in the position and intensity of the southern westerly wind belt. Nat. Geosci. 695–699.
Long, C.J., Whitlock, C., Bartlein, P.J., Millspaugh, S.H., 1998. A 9000-year fire history from the Oregon Coast Range, based on a high-resolution charcoal study. Can. J. For. Res. 28, 774–787.
Lynch, A.H., Beringer, J., Kershaw, P., Marshall, A., Mooney, S., Tapper, N., Turney, C., van der Kaars, S., 2007. Using the paleorecord to evaluate climate and fire interactions in Australia. Earth Planet. Sci. Lett. 35, 215–239.
Macphail, M.K., 1979. Vegetation and climates in southern Tasmania since the last glaciation. Quat. Res. 11, 306–341.
Markgraf, V., Whitlock, C., Haberle, S., 2007. Vegetation and fire history during the last 18,000 cal yr BP in southern Patagonia: Mallín Pollux, Coyhaique, Province Aisén (45 41′ 30 ″S, 71 50′ 30 ″W, 640 m elevation). Palaeogeogr. Palaeoclimatol. Palaeoecol. 254, 492–507.
Marx, S.K., McGowan, H.A., Kamber, B.S., 2009. Long-range dust transport from eastern Australia: a proxy for Holocene aridity and ENSO-type climate variability. Earth Planet. Sci. Lett. 282, 167–177.
McGlone, M.S., Wilmshurst, J.M., 1999. Dating initial Maori environmental impact in New Zealand. Quat. Int. 59, 5–16.
McGlone, M.S., Salinger, M.J., Moar, N.T., 1993. Paleovegetation studies of New Zealand's climate since the last glacial maximum. In: Wright Jr., H.E., Kutzbach, J.E., Webb III, T., Ruddiman, W.F., Street-Perrot, F.A., Bartlein, P.J. (Eds.), Global Climates since the Last Glacial Maximum. University of Minnesota Press, Minneapolis, MN, pp. 294–317.
Meneghini, B., Simmonds, I., Smith, I.N., 2007. Association between Australian rainfall and the southern annular mode. Int. J. Climatol. 27, 109–121.
Moreno, P.I., Francois, J.P., Moy, C.M., Villa-Martinez, R., 2010. Covariability of the Southern Westerlies and atmospheric CO2 during the Holocene. Geology 38, 727–730.
Moy, C.M., Seltzer, G.O., Rodbell, D.T., Anderson, D.M., 2002. Variability of El Niño/Southern oscillation activity at millennial timescales during the Holocene epoch. Nature 420, 162–165.
Moy, C.M., Dunbar, R.B., Guilderson, T.P., Waldmann, N., Mucciarone, D.A., Recasens, C., Ariztegui, D., Austin Jr., J.A., Anselmetti, F.S., 2011. A geochemical and sedimentary record of high southern latitude Holocene climate evolution from Lago Fagnano, Tierra del Fuego. Earth Planet. Sci. Lett. 302, 1–13.
Nicholls, N., Lucas, C., 2007. Interannual variations of area burnt in Tasmanian bushfires: relationships with climate and predictability. Int. J. Wildland Fire 16, 540–546.
Norton, K.P., Blanckenburg, F., 2010. Silicate weathering of soil-mantled slopes in an active Alpine landscape. Geochim. Cosmochim. Acta 74, 5243–5258.
Osok, R., Doyle, R., 2004. Soil development on dolerite and its implications for landscape history in southeastern Tasmania. Geoderma 121, 169–186.
Page, M.J., Trustrum, N.A., DeRose, R.C., 1994. A high resolution record of storm-induced erosion from lake sediments, New Zealand. J. Paleolimnol. 11, 333–348.
Quigley, M.C., Horton, T., Hellstrom, J.C., Cupper, M.L., Sandiford, M., 2010. Holocene climate change in arid Australia from speleothem and alluvial records. Holocene 20, 1093–1104.
R Core Team, 2014. R: a Language and Environment for Statistical Computing. R Foundation for Statistical Computing, Vienna, Austria. URL. http://www.R-project.org/.
Rees, A.B.H., Cwynar, L.C., 2010. Evidence for early postglacial warming in Mount Field National Park, Tasmania. Quat. Sci. Rev. 29, 443–454.
Rees, A.B.H., Cwynar, L.C., Cranston, P.S., 2008. Midges (Chironomidae, Ceratopogonidae, Chaoboridae) as a temperature proxy: a training set from Tasmania, Australia. J. Paleolimnol. 40, 1159–1178.
Rodbell, D.T., Seltzer, G.O., Anderson, D.M., Abbott, M.B., Enfield, D.B., Newman, J.H., 1999. An ~15,000-year record of El Niño-driven alluviation in southwestern Ecuador. Science 22, 516–520.
Sandweiss, D.H., Richardson III, J.B., Reitz, E.J., Rollins, H.B., Maasch, K.A., 1996. Geoarchaeological evidence from Peru for a 5000 years B.P. onset of El Niño. Science 13, 1531–1533.
Shulmeister, J., Lees, B.G., 1995. Pollen evidence from tropical Australia for the onset of an ENSO-dominated climate at c. 4000 BP. Holocene 5 (1), 10–18.
Shulmeister, J., Goodwin, I., Renwick, J., Harle, K., Armand, L., McGlone, M.S., Cook, E.J., Dodson, J.R., Mayewski, P., Curran, M., 2004. The Southern Hemisphere westerlies in the Australasian sector over the last glacial cycle: a synthesis. Quat. Int. 118–119, 23–53.
ter Braak, C.J.F., Šmilauer, P., 2002. CANOCO version 4.5. Biometris-Plant Research International, Wageningen.
Tiller, K.G., 1963. Weathering and soil formation on dolerite in Tasmania with particular reference to several trace elements. Aust. J. Soil Res. 1, 74–90.
Toggweiler, J.R., 2009. Shifting westerlies. Science 323, 1434–1435.
Toggweiler, J.R., Russell, J.L., Carson, S.R., 2006. Midlatitude westerlies, atmospheric CO_2, and climate change during the ice ages. Paleoceanography 21, PA2005.
Tyler, L.D., McBride, M.B., 1982. Mobility and extractability of cadmium, copper, nickel, and zinc in organic and mineral soil columns. Soil Sci. 134, 198–205.
Walker, I.R., Smol, J.P., Engstrom, D.R., Birks, H.J.B., 1991. An assessment of Chironomidae as quantitative indicators of past climatic change. Can. J. Fish. Aquat. Sci. 48, 975–987.
Walsh, M.K., Pearl, C.A., Whitlock, C., Bartlein, P.J., Worona, M.A., 2010. An 11 000-year-long record of fire and vegetation history at Beaver Lake, Oregon, central Willamette Valley. Quat. Sci. Rev. 29, 1093–1106.
Whitlock, C., Moreno, P.I., Bartlein, P., 2007. Climatic controls of Holocene fire patterns in southern South America. Quat. Res. 68, 28–36.
Wiederholm, T., 1983. Chironomidae of the Holarctic region. Keys and diagnoses, Part 1: larvae. Entomol. Scand. (Suppl. 19)
Williams, A.A.J., Karoly, D.J., 1999. Extreme fire weather in Australia and the impact of the El Nino southern Oscillation. Aust. Meteorol. Mag. 48, 15–22.
Wright Jr., H.E., 1991. Coring tips. J. Paleolimnol. 6, 37–49.
Wright Jr., H.E., Mann, D.H., Glaser, P.H., 1984. Piston corers for peat and lake sediments. Ecology 65, 657–659.
Xia, Q.K., Zhao, J.-X., Collerson, K.D., 2001. Early-mid Holocene climatic variations in Tasmania, Australia: multi-proxy records in a stalagmite from Lynds Cave. Earth Planet. Sci. Lett. 194, 177–187.